Natural Resources Canada | Ressources naturelles Canada

NATURAL RESOURCES CANADA – INVENTIVE BY NATURE

Canadian Chromite R&D Initiative

Chapter 3.2.1

Direct Reduction of Chromite Conceptual Approach and Overview

Dogan Paktunc

CanmetMINING, 555 Booth Street, Ottawa, ON, K1A 0G1
dogan.paktunc@canada.ca

September 2021

This work was completed through funding provided by Natural Resources Canada as part of the Canadian Rare Earth Element and Chromite R&D Initiative.

Chapter 3.2.1

Direct Reduction of Chromite

Conceptual Approach and Overview

Dogan Paktunc

CanmetMINING, 555 Booth Street, Ottawa, ON, K1A 0G1

dogan.paktunc@canada.ca

ABSTRACT

Direct reduction of chromite (DRC) process is production of ferrochrome from chromite ore at temperatures much lower than those typical of smelting in electric arc furnaces with the overall aim of reducing energy consumption and production costs. This is achieved with the use various fluxes like NaOH, cryolite (Na_3AlF_6) and $CaCl_2$ and without melting the feed. In the case of $CaCl_2$ flux, carbothermic reduction of ground chromite at 1300 °C for 2 hours typically results in an M_7C_3 type carbide having the average composition of $Cr_{4.7}Fe_{2.3}C_3$ corresponding to over 94% Cr and 100% Fe metallization. The slag is dominantly made of refractory spinel, which is essentially $MgAl_2O_4$. Recovery of ferrochrome from the final DRC products is achieved by conventional mineral processing techniques such as gravity and magnetic separation. During the early stages of reduction until about 1100 °C, exchange reactions are dominated by increases in the $Mg/(Mg+Fe^{2+})$ ratio and slight increases in the $Cr/(Cr+Al+Fe^{3+})$ ratio of chromite until about 10 to 20 % Fe^{2+} remaining in the tetrahedral sites. This is the onset of Cr reduction with continual and significant losses of Cr until about 1200 °C where there is approximately 30% Cr remaining in the octahedral sites. At this point, all Fe is reduced and the remaining Cr is reduced, leaving behind Mg-Al spinel. In melt, Cr is reduced to Cr^{2+} and transported as monomeric species of CrO in a four-fold coordination. The mechanism of the direct reduction involves incongruent dissolution of chromite, mass transport of dissolved Cr and Fe species as ionic species in molten media and their reduction on carbon particles as an M_7C_3 type carbide. The dissolution reactions on chromite surfaces and formation of alloy on carbon particles occur simultaneously with the latter being faster. Oxygen partial pressures are around $1x10^{-11}$ atm near the dissolving chromite and $1x10^{-16}$ atm near the carbon particles. These are the driving forces of transporting Fe and Cr species in molten salt by creating concentration gradients between chromite and carbon particles. As the chromite and carbon particles shrink, the melt remains undersaturated with respect to Fe and Cr for the reactions to continue.

INTRODUCTION

Direct reduction of chromite (DRC) process can be defined as the production of a metallic ferrochrome from chromite ore using a carbon reductant and a flux without melting the whole feed. It differs from smelting in electric arc furnaces where the whole feed is melted and ferrochrome in liquid form is separated from the liquid slag by tapping of density segregated molten materials. In the case of DRC, the final products are solid and the physical separation is accomplished by conventional mineral processing techniques such as gravity and magnetic separation.

The need for value-added downstream products from mining the ore is an important sustainability driver as discussed in Chapter 1.1 (Paktunc 2021). In addition, energy efficient and low-carbon processes are critical for the new economy and for the competitiveness of the Canadian mining industry in the world markets.

Ferrochrome production from chromite requires the breakage of the strong Cr and oxygen bonds and reduction of trivalent Cr species in the ore to zero-valent Cr as in ferrochrome. Total energy needed to break the Cr-O bonds is much greater than the energy needed for making Cr-Cr or metal to metal and carbon bonds; therefore, the enthalpy of this reaction is high. In other words, the reaction is highly endothermic requiring energy for this reaction to proceed.

Over 80% of the world's ferrochrome production is made by submerged arc furnaces, about 10% is produced by Glencore's Premus technology and around 6% is by DC arc furnaces. Ferrochrome smelting in electric arc furnaces is energy intensive with the slag melting and tapping temperatures exceeding 1700 °C. Temperatures at the tip of the graphite electrodes reaching and exceeding 2000 °C for the submerged arc furnaces and much higher for the DC arc furnace. Energy requirements of smelting can exceed 4 MWh per ton Cr in ferrochrome produced. In addition, greenhouse gas emissions related to smelting in electric arc furnaces can exceed 10 t CO_2 per ton Cr in ferrochrome produced (International Chromium Development Association 2016). Among the most advanced smelting technologies, the lowest energy consumptions are recorded for Glencore's Premus technology, which utilizes rotary kilns for pre-reduction of the pellets ahead of smelting. Reductions in energy consumption are about one third of the specific energy consumption. Pre-reduction technology involves partial reduction of chromite mixed with a reductant in pellets prior to smelting in an electric arc furnace. Over a three-decade period, pre-reduction of chromite has been the topic of many studies as summarized by Paktunc et al. (2018). The fluxes included NaCl, NaF, CaF_2, NaF, K_2CO_3, CaO, MgO, Al_2O_3, SiO_2, borates and granite. KWG Resources filed a patent on direct reduction of chromite with the use of natural gas and several alkalis as the accelerants (Winter 2015; Barnes et al. 2015).

These issues and studies formed the motivation for our research under the Chromite R&D initiative. Based on the need for alternate reduction technologies and the gaps in knowledge (Hatch 2016), the project has focused on innovation through the generation of new knowledge with the following main objectives: (1) developing a fundamental-level understanding of carbothermic reactions and evolution of Cr and Fe species during reduction, (2) identification of clean and technologically most advanced flow sheets, and (3) developing an alternate ferrochrome technology with lower energy consumptions and lower greenhouse gas emissions leading to the design of a flow sheet for a "made-in Canada" ferrochrome facility.

CONCEPTUAL APPROACH

Thermodynamic simulations and exploratory experiments on carbothermic reduction of chromite at around 1300 °C using several alkali fluxes indicated the presence of molten media and that in-situ reduction and metallization of Cr and Fe species occur on carbon particles. A review and screening of the potential fluxes with melting points less than the target reduction temperature of 1300 °C and boiling points greater than 1300 °C identified several candidate fluxes that can provide a medium for transporting the reducible cations, Fe and Cr. Fluxes with high boiling points would have lower potential for evaporation during reduction. Examples of fluxes meeting these criteria include NaCl (melts at ~800 °C; boils at 1413 °C), $CaCl_2$ (melts at ~770 °C; boils at 1935 °C) and Na_3AlF_6 (melts at 1012 °C).

Possible reduction reactions of Fe and Cr involving C and CO are listed below along with their enthalpy changes at 298 K.

$FeO + CO \rightarrow Fe + CO_2$ ΔH_{298K}= -17.2 kJ (1)

This reaction proceeds instantaneously as it requires little or no heat. In contrast, reduction of FeO with solid carbon begins at 725 °C, represented by the following reaction (Fig. 1).

$FeO + C \rightarrow Fe + CO$ ΔH_{298K}= 155.3 kJ (2)

Another possibility is the formation of cementite (Fe_3C) as the alloy product from the reduction of FeO with carbon.

$3\ FeO + 4\ C \rightarrow Fe_3C + 3\ CO$ ΔH_{298K}= 491.1 kJ (3)

$Fe_2O_3 + 3\ C \rightarrow 2\ Fe + 3\ CO$ ΔH_{298K}= 494.2 kJ (4)

$FeCr_2O_4 + C \rightarrow Fe + Cr_2O_3 + CO$ ΔH_{298K}= 220.5 kJ (5)

$3\ FeCr_2O_4 + 4\ C \rightarrow Fe_3C + 3\ Cr_2O_3 + 3\ CO$ ΔH_{298K}= 686.6 kJ (6)

$FeCr_2O_4 + CO \rightarrow Fe + Cr_2O_3 + CO_2$ ΔH_{298K}= 48.0 kJ (7)

A comparison of the reactions 3 and 6 indicates that reduction of FeO to cementite requires less heat than chromite. Whereas the reduction of chromite to cementite begins at 1047 °C, reduction of FeO to cementite occurs at much lower temperatures beginning at 728 °C (Fig. 1).

Reduction of Cr_2O_3 by carbon to Cr_3C_2, Cr_7C_3 or Cr is possible at temperatures that are greater than 1128, 1140 and 1253 °C, respectively (Fig. 1). The reactions 8 to 12 are highly endothermic. Reduction of Cr_2O_3 by CO (Reaction 12) is not realistic because its standard Gibbs free energy values are in the 1840 to 2237 kJ range at 1200 to 1600 K.

$3\ Cr_2O_3 + 13\ C \rightarrow 2\ Cr_3C_2 + 9\ CO$ ΔH_{298}= 2243.8 kJ (8)

$7\ Cr_2O_3 + 27\ C \rightarrow 2\ Cr_7C_3 + 21\ CO$ ΔH_{298}= 5289.1 kJ (9)

$Cr_2O_3 + 3\ C \rightarrow 2\ Cr + 3\ CO$ ΔH_{298}= 795.5 kJ (10)

$7\ MgCr_2O_4 + 27\ C \rightarrow 2\ Cr_7C_3 + 7\ MgO + 21\ CO$ ΔH_{298K}= 5586.4 kJ (11)

$7\ Cr_2O_3 + 33\ CO \rightarrow 2\ Cr_7C_3 + 27\ CO_2$ $\Delta H_{298K} = 632.5$ kJ (12)

Reduction of magnesiochromite ($MgCr_2O_4$) occurs at temperatures that are above 1248 °C (Fig. 1). Similar to its counterpart in Fe, this is about 100 °C higher than the reduction of Cr_2O_3 to Cr_7C_3 in that reduction of Cr in chromite is more difficult than it is in the form of Cr_2O_3. Along with the enthalpy changes these indicate that reduction of Cr_2O_3 and FeO are thermodynamically favorable to reduction of chromite. In this case, it will be advantageous to have Cr_2O_3 and FeO as the reactants rather than chromite. Incongruent dissolution of chromite resulting in the release of Cr and Fe as oxides to molten media followed by their reduction as simple oxides provide an explanation for the ease at which Cr and Fe are reduced via direct reduction. This rationalized the research on direct reduction of chromite while forming a motivation for an in-depth understanding of the mechanism.

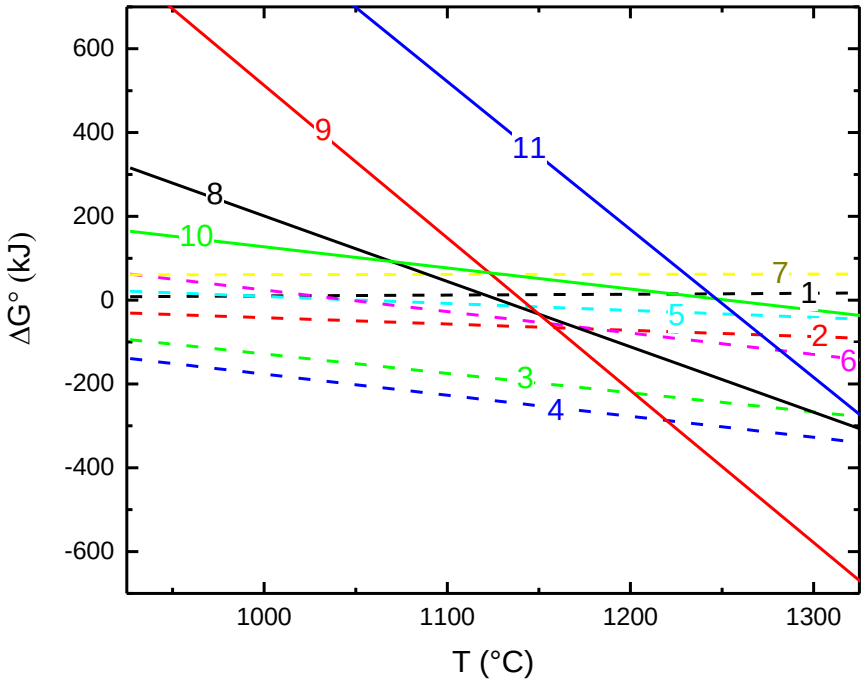

Figure 1. Standard Gibbs free energy of the reduction reactions involving Fe (1) to (7) and Cr species (8) to (11). Reaction 12 with very high ΔG° values plot outside of the graph.

Experimental studies using such fluxes were designed with the objectives of achieving fast reduction kinetics, high metallization and alloy growth. The experimental design considered ore composition and particle size, reductant types and particle sizes, flux concentrations and the form of feed (i.e. loose particulate vs pelletized feed). The products were characterized by advanced techniques such as quantitative mineralogy, and synchrotron-based X-ray absorption spectroscopy and high-energy X-ray diffraction. The results as summarized below indicated that direct reduction of chromite in the presence of a flux meeting the above criterion was possible at about 1300 °C.

Ferrochrome formed through direct reduction processes is considered to have a much higher energy efficiency through decreasing reduction temperatures to about 1300 °C with reaction durations of approximately 2 hours. An underlying premise with the direct reduction process is that the ferrochrome is separated from the gangue by physical means like using simple mineral processing techniques involving comminution followed by gravity and/or magnetic separation.

These findings provided an engineering or process opportunity with a conceptualization of the mechanism of the DRC process with the premise that chromite dissolved incongruently, releasing Fe and Cr to melt and leaving behind $MgAl_2O_4$ as a residue.

ALKALI-ASSISTED DRC PROCESS

Studies on the use of several alkalis as the accelerants and the patent known as the KWG process (Winter, 2015; Barnes et al., 2015) indicated that NaOH addition improved both the reaction rate and extent of reduction at temperatures lower than those that are typical of conventional smelting technologies.

Our studies on direct reduction of a chromite ore with alkali fluxes at 1300 °C after 1h of reaction resulted in the formation of $(Cr,Fe)_7C_3$ type alloys with degrees of Cr metallization varying from 45% for NaCl to 85 % for NaOH. The degree of metallization for the Na_2CO_3 flux was in between at 66% Cr. The feed was composed of 74.6 wt% Ring of Fire chromite ore, 16.4 wt% carbon and 9 wt% flux with the resulting alloy compositions of $Cr_{3.2\text{-}5.0}Fe_{2.0\text{-}3.8}C_3$ for NaCl, $Cr_{3\text{-}4}Fe_{3\text{-}4}C_3$ for Na_2CO_3 and $Cr_{4.2\text{-}4.9}Fe_{2.1\text{-}2.8}C_3$ for NaOH. Alkali-assisted direct reduction facilitated the formation of a liquid slag needed for transporting Fe and Cr from chromite to reductant particles. Crystallization of $NaAlO_2$ during slag formation between 800 and 1300 °C restricted the transport or diffusion of the reducible cations in molten slag. At temperatures above 1300 °C, $NaAlO_2$ decomposes resulting in an increase of the liquid slag while aiding the formation of the refractory Mg-Al spinel. In the case of NaCl, the reason for the observed low degrees of metallization was in part due to the evaporation of NaCl at around 1150 °C. Ferrochrome particles formed were often small and largely unliberated, which would make the physical recovery of ferrochrome challenging. The increased amount of liquid slag at 1400 °C aided the growth of alloy particles.

With the degree of Cr metallization at 85%, direct reduction of chromite aided by NaOH is promising as an alternate technology to that of smelting in electric arc furnaces. The details of the alkali-assisted DRC process were summarized in Paktunc et al (2018) and Sokhanvaran et al (2018).

CRYOLITE-ASSISTED DRC PROCESS

Cryolite (Na_3AlF_6) which is widely used as an electrolyte in the production of aluminum has a high solubility for oxides like Al_2O_3. Similar to the alkalis, addition of cryolite as a flux to the ore and reductant mixture accelerated the kinetics of reduction and resulted in the formation of coarse ferrochrome alloy particles with an average composition of $Cr_5Fe_2C_3$. The use of cryolite enabled the formation of a liquid layer around chromite particles to allow mass transport of reducible cations. With the use of a feed that is composed of 65.4 wt% Ring of Fire chromite ore, 15 wt% carbon and 19.6 wt% cryolite, over 93% Cr metallization is achieved after 2 hours of reduction at 1300 °C. The large particle size of the alloy phase and its density difference from the slag make the separation and recovery possible by simple gravity techniques.

Cryolite can be substituted by the solid wastes produced at Al smelters that are known as secondary cryolite, crushed bath, bath cryolite and pure bath material. Although the bath material is recycled by the Al industry, a portion of it is disposed of as waste, which creates an opportunity for its reutilization. The details of this process were provided in Sokhanvaran and Paktunc (2019).

CALCIUM CHLORIDE-ASSISTED DRC PROCESS

$CaCl_2$-assisted DRC process involves incongruent dissolution of chromite in molten $CaCl_2$ followed by the reduction of the Fe and Cr species in solution on solid carbon particles (Yu and Paktunc 2018b,c). The process requires that parameters such as the proportions of the ore, reductant and $CaCl_2$ in the pellet, and their particle sizes are optimized for efficient reduction kinetics and product quality. Ore composition with respect to the concentrations of Cr_2O_3, Fe_2O_3 and FeO is important for determining the amount of the reductant. Particle sizes influence the reaction rates and final product quality. The proportion of $CaCl_2$ is also critical for the reaction rates. In addition, factors such as pellet porosity or compactness and the distribution of the reactant particles in the pellets are important.

Studies indicated that the pellets that are made of 100 parts ore, 20 parts reductant and 25 or 30 parts $CaCl_2$ by mass are reasonable for a typical Ring of Fire chromite ore (Yu and Paktunc 2018a, 2018b, 2018c; Carter et al., 2021; Coumans et al., 2021). The amount of the reductant is slightly greater than the stoichiometric carbon to maintain the partial pressures of CO/CO_2 as per the Boudouard equilibrium. Ore particles that are in the -107+75 μm size range are mixed with a reductant having the same particle size range and $CaCl_2$ that is finer than about 35 μm. The reductant is preferably reactive and having high fixed carbon with low volatile content. Petcoke meets this criterion as it has performed well during the experiments, with the formation of alloy products that are similar to those of graphite experiments. The feed is pelletized using a drum pelletizer with the nominal size of pellets being approximately 12 mm across.

The feed in the form of pellets is reduced at 1300 °C for 2 hours under an inert atmosphere. This typically results in over 94% Cr and 100% Fe metallization in the form of discrete particles of ferrochrome that measure several hundred microns, as illustrated in Figure 2. Ferrochrome is an M_7C_3 type carbide having the average composition of $Cr_{4.7}Fe_{2.3}C_3$. The Cr/Fe molar ratio of this carbide is close to its original value in chromite suggesting that Cr reduction was efficient with excellent Cr and Fe recoveries. The slag is dominantly made of refractory spinel measuring several hundred microns across. It is essentially $MgAl_2O_4$ but it can contain trace to minor amounts of Cr. Spinel particles are porous with a sponge-like texture. The particles are less than about 100 μm across which are similar to the original size of chromite particles in the feed (i.e. -107+75 μm).

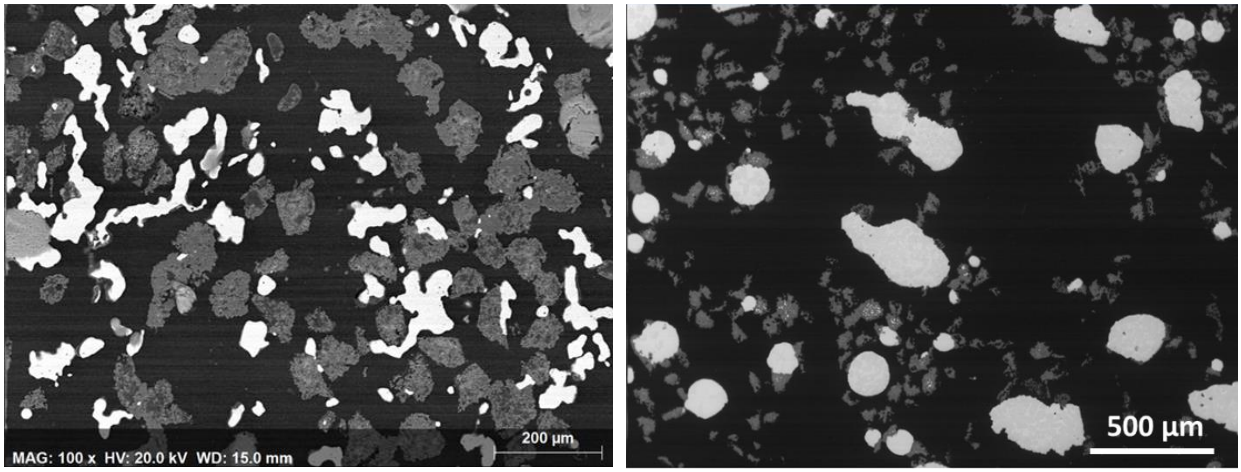

Figure 2. Backscattered electron micrographs showing products resulting from $CaCl_2$-assisted direct reduction at 1300 °C for 2 hours. White particles are FeCr alloy occurring as coarse and discrete particles separated from the residual spinel (slag) particles (gray). Slag particles on the left photomicrograph are retaining the original chromite particle sizes.

In addition to forming discrete M_7C_3-type carbide particles, Fe occurs within chromite in the form of minute or plate-like metallic particles following the crystallographic planes of chromite (Fig. 3). Such occurrences are minor; however, their presence suggests that CO reduces some FeO. This observation can be explained by spontaneous Reaction 1, as described earlier. In some samples, metallic Fe particles have minor Cr, which is problematic, because reduction of Cr_2O_3 by CO (Reaction 12) is unlikely due to the extremely high enthalpy change for this reaction.

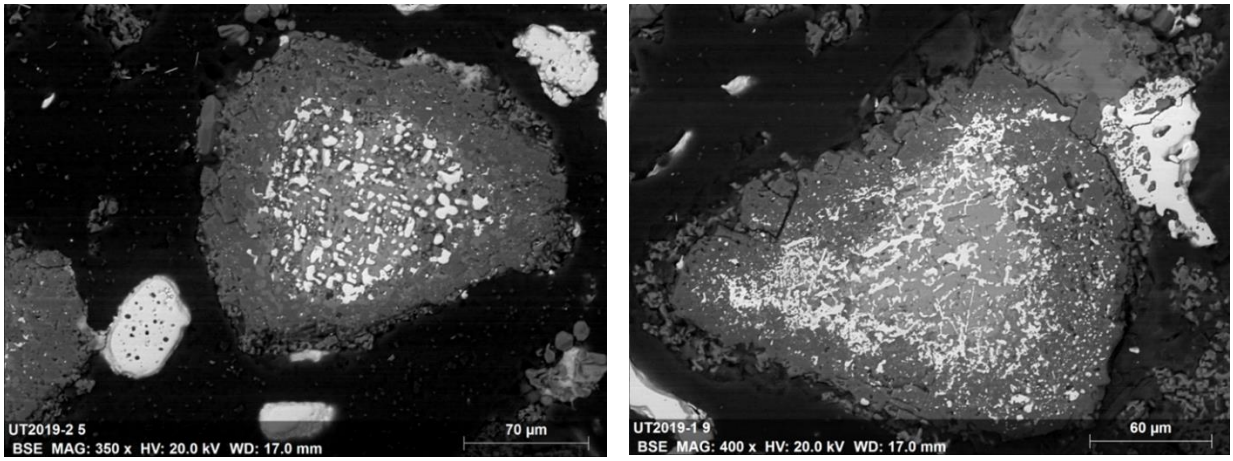

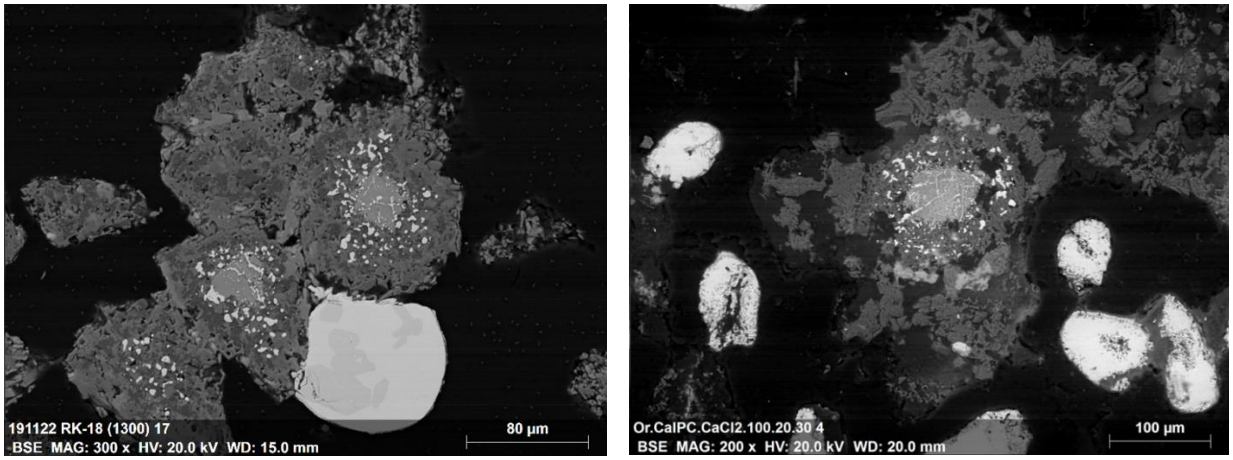

Figure 3. Fe-rich alloy particles (white) forming in-situ within chromite particles in the form of small blebs and plate-like particles following the crystallographic planes of the host chromite/spinel particle (grey). Light grey is residual chromite and dark grey areas are refractory spinel. Alloy particles in residual chromite are Fe-rich in comparison to those that occur as isolated large particles, which are M_7C_3-type carbides.

As illustrated in Figure 4, Cr_2O_3 reduction (reaction 13) has ΔG° values that are lower by approximately 200 kJ than the CO-CO_2 equilibrium (14) across the temperature interval of interest. In comparison, the C-CO equilibrium (15) intersects the Cr_2O_3-Cr reaction at about 1250 °C confirming the need for solid carbon for Cr_2O_3 reduction. At very high partial pressures of CO where P_{CO}/P_{CO2} is greater than about 1500, thermodynamics predict reduction of Cr_2O_3 by CO at temperatures of around 1300 °C (Fig. 4). As discussed by Yu and Paktunc (2018b) and Sokhanvaran and Paktunc (2017), very low oxygen partial pressures such as ~10^{-12} atm can be attained locally with finely distributed carbon in close proximity to chromite. Because pellets behave like mini reactors during direct reduction, excess carbon maintains high P_{CO}/P_{CO2} within pellets. In this case, as long as the Boudouard equilibrium (16) is maintained with excess C within mini reactors (pellets), reduction processes will be aided by CO for not only reducing FeO but also Cr_2O_3.

$$4/3\ Cr + O_2 \rightarrow 2/3\ Cr_2O_3 \quad (13)$$

$$2\ CO + O_2 \rightarrow 2\ CO_2 \quad (14)$$

$$2\ C + O_2 \rightarrow 2\ CO \quad (15)$$

$$C + CO_2 \rightarrow 2\ CO \quad (16)$$

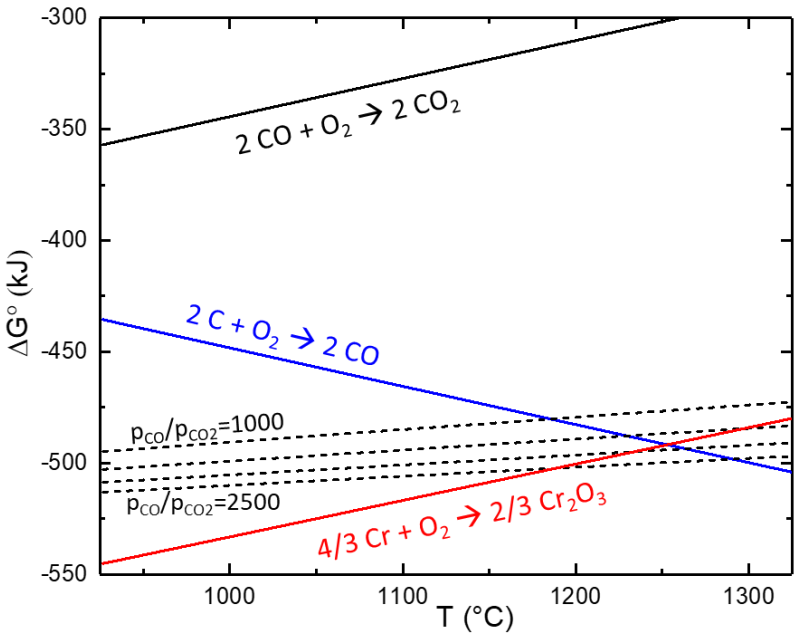

Figure 4. Influence of partial pressures of CO and CO_2 on the reducibility of Cr_2O_3. Dashed lines are CO-CO_2 equilibrium under non-standard conditions with P_{CO}/P_{CO2} values of 1000, 1500, 2000 and 2500.

The overall reduction of chromite can be represented by the following reaction where the feed composition is the average composition of the Ring of Fire chromite based on over 2000 electron microprobe analyses (Paktunc 2021).

$$Mg_{0.4}Fe_{0.6}Cr_{1.4}Al_{0.6}O_4 + 3.5\ C \rightarrow 0.2\ Cr_7C_3 + 0.2\ Fe_3C + 0.3\ MgAl_2O_4 + 0.1\ MgO + 2.7\ CO \qquad (17)$$

In this case, one mole of chromite is reacting with 3.5 moles C to form a M_7C_3 type carbide, spinel, MgO and CO. The solid products are equal molar proportions of combined Cr- and Fe-carbide alloys and slags as refractory spinel and MgO. This reaction will be slightly different when the presence of gangue minerals in the feed is considered.

In terms of the degrees of metallization, synchrotron X-ray absorption near edge structure (XANES) spectroscopy indicated that the degrees of Fe metallization were 91.6% at 1200 °C and 100% at 1300 °C (Yu and Paktunc 2018c). The degrees of Cr metallization were 58.6% at 1200 °C, 94.2% at 1300 °C and 100% at 1400 °C.

Reaction kinetics

The off-gas data from TGA and furnace experiments indicate that the reactions begin at around 500 °C with the decomposition of clinochlore as the dominant gangue mineral, followed by melting of $CaCl_2$ at 760 °C. These are closely followed by the reduction of Fe beginning at around 800 °C. The changes in the measured CO concentrations in the off-gas are rapid once the reduction reactions begin (Fig. 5). Integration of the CO peak indicates that the bulk of the reduction takes place within about 1 hour for small-scale tests and about 2 hours for the large-scale tests. In some of the large-scale tests, the reduction reactions appear to slow down between about 1200 °C and the peak temperature of 1300 °C. This change

in reduction rate may be indicative of the onset of endothermic Cr reduction reactions that are discernable in large-scale experiments due to heat transfer limitations.

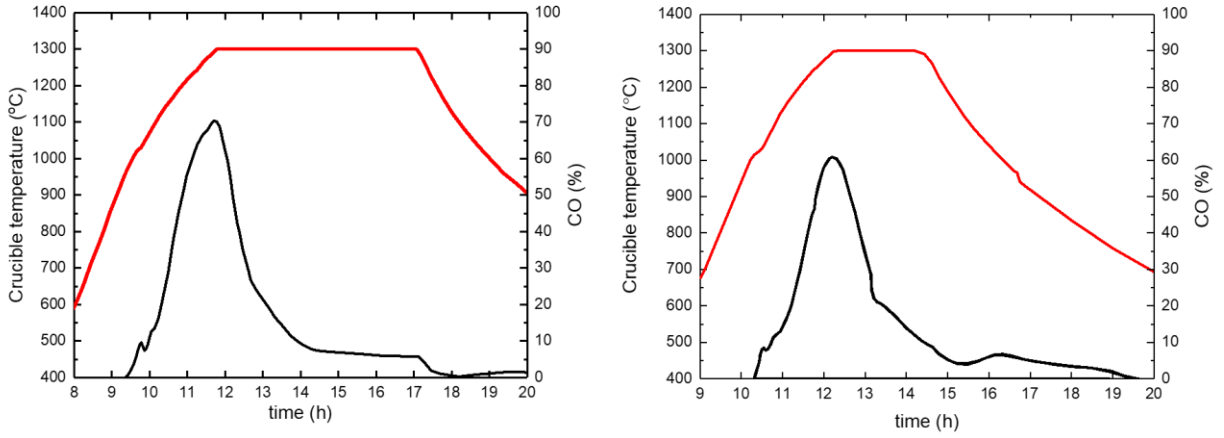

Figure 5. Typical off-gas data showing the evolution of CO concentrations (black) and temperatures (red) with time during 2 large-scale reduction tests with 5 hours (left) and 2 hours (right) retention times at 1300 °C.

Thermodynamics of the process

Assuming that the reactants are made of 61.4 wt% ore, 16.3 wt% carbon and 22.3 wt% $CaCl_2$, thermodynamic calculations indicate that the flux, $CaCl_2$ remains molten across the 800 to 1400 °C range. There are gradual decreases in the equilibrium compositions of chromite and carbon across the temperature interval of 800 to 1100 °C (Fig. 6). Accompanying these changes are gradual increases in the CO and alloy contents of the products. The compositional changes in the equilibrium end-products are drastic in the 1100-1200 °C range and more gradual from 1200 to 1300 °C. These observations are consistent with the off-gas data from furnace experiments discussed earlier and the results of Coumans et al. (2021).

Thermodynamics predict that mass losses of about 1.8 % at 900 °C, increasing to 3.9 % at 1000 °C and 9.7 % at 1100 °C. At 1200 °C and above, the mass losses are greater than about 20 %. The changes in the equilibrium compositions of chromite from 800 to 1400 °C are shown in Figure 6. The $MgCr_2O_4$ end-member rapidly increases across the 800 to 1100 °C range. This occurs at the expense of $FeCr_2O_4$ and $FeAl_2O_4$ end-members suggesting that Fe is reduced across this temperature range. The $MgCr_2O_4$ end-member begins to rapidly decrease above 1100 °C. This is due to the loss of Cr from the spinel structure. Overall, these are decreases in the equilibrium proportions of the Cr- and Fe-end members of chromite from 800 to 1300 °C, leaving behind the end members that are refractory. Mg-Al spinel concentrations increase rapidly above 1100 °C and reach a maximum value at 1400 °C. At 1300 °C, there is still about 3-4 % $MgCr_2O_4$ remaining, so reduction reactions are not 100 % complete at 1300 °C, indicating that the recovery of Cr is not kinetically limited at 1300 °C. These are consistent with the empirical data and observed compositions of the residual chromite or spinel in the final products, suggesting that the equilibrium is reached or very close by the end of the experiments at 1300 °C.

Thermodynamic calculations indicate that the reduced Fe occurs as an FCC-type compound at 800 to 1000 °C. It forms about 5 wt% of the products at 1000 °C. Beginning at 1100 °C, Cr occurs as an M_7C_3 type compound dominated by Fe (i.e. $Cr_{2.3}Fe_{4.7}C_3$). It quickly evolves to a Cr-dominated carbide at 1200 °C, which is similar in composition to the one observed in products resulting from reduction at 1300 °C (i.e. $Cr_{4.7}Fe_{2.3}C_3$). This is close to the equilibrium composition of $Cr_{4.9}Fe_{2.1}C_3$, suggesting near-equilibrium conditions after 2 hours of reduction at 1300 °C.

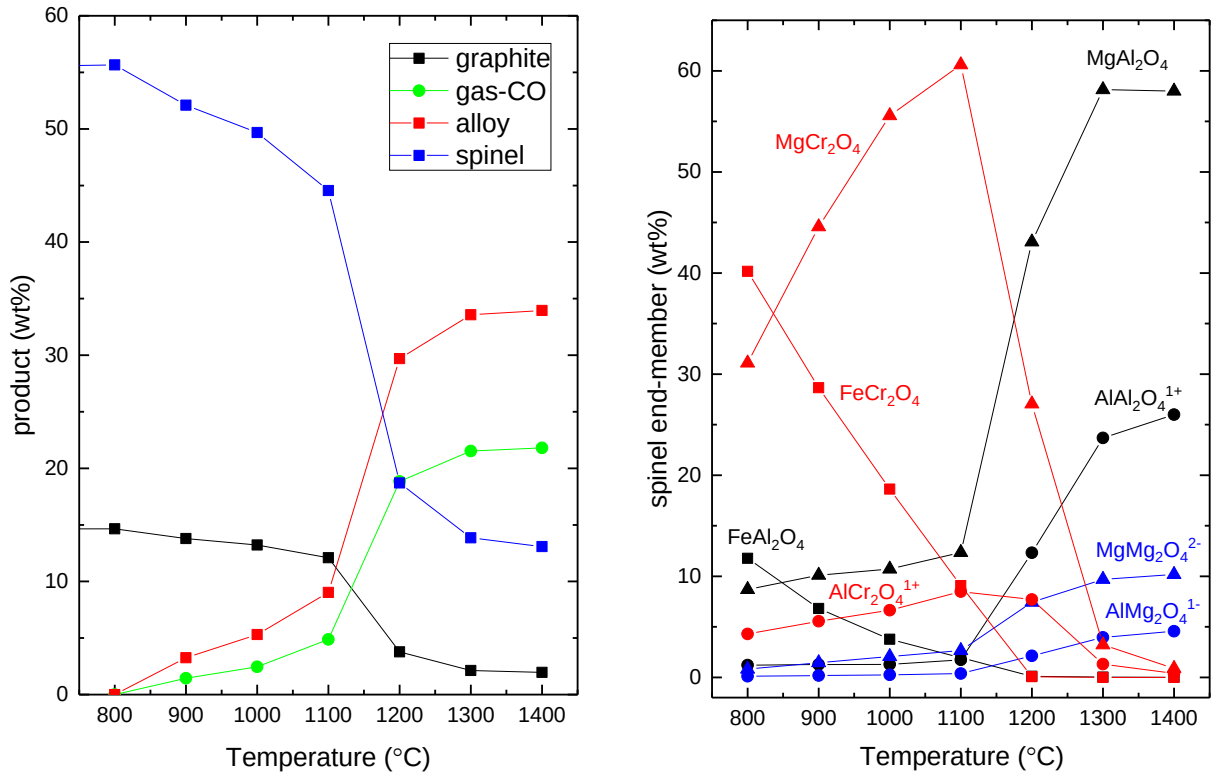

Figure 6. Predicted equilibrium compositions of the reactants and products (a) and proportions of the spinel/chromite end members (b) at the temperature range of 800 to 1400 °C.

In order to better understand the reduction reactions, and influence and role of $CaCl_2$ flux on the distribution of cations in the chromite/spinel structure, thermodynamic simulation of the ore, reductant and $CaCl_2$ mixture made earlier was repeated for (1) ore, (2) ore and carbon, and (3) ore and $CaCl_2$ at temperatures of 800 to 1400 °C (Fig. 7). Distribution patterns of the tetrahedral and octahedral cations are similar for ore and ore+$CaCl_2$, and for ore+carbon and ore+carbon+$CaCl_2$, indicating the role of $CaCl_2$ flux as a catalyst only. In the absence of a reductant, high temperature reactions are limited to Mg-Fe^{2+} exchange reactions at tetrahedral sites. These are gradual decreases in Fe^{2+} and increases in Mg as the temperature increases from 800 to 1300 °C. Changes in the Cr and Al concentrations are limited at this temperature range. The same is true for Cr and Al in the presence of $CaCl_2$ flux; however, $CaCl_2$ seems to influence Mg-Fe^{2+} exchange reactions in that at temperatures less than about 1150 °C, Mg partitions to the melt whereas Fe partitions to chromite. This is reversed at temperatures greater than about 1150 °C.

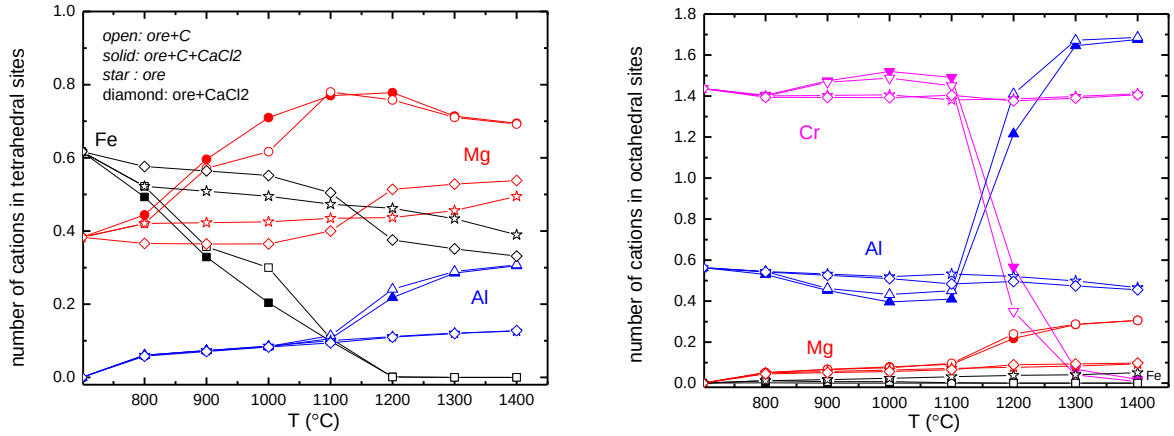

Figure 7. Equilibrium compositions in terms of cation distribution in tetrahedral and octahedral sites of chromite across the temperature range of 800 to 1400 °C for starting compositions of ore, reductant and $CaCl_2$ flux (solid symbols), ore and reductant (open symbols), ore and $CaCl_2$ flux (diamond), and ore only (star)

In the presence of carbon and $CaCl_2$, chromite heated to 1300 °C with no dwell time is compositionally similar to the original chromite indicating that reduction and Mg-Fe^{2+} exchange reactions were limited to the margins of chromite particles (Fig. 8) whilst interiors of chromite were not affected. In contrast, chromite reacted with $CaCl_2$ for 3 hours at 1300 °C resulted in substantial loss of Fe^{2+} from its interiors. This was not due to core to rim Mg-Fe^{2+} exchange reactions because core to rim variations involve mainly trivalent cations, indicating that FeO is released to the melt. Compositional variation in terms of the Mg/(Mg+Fe^{2+}) ratio, which is restricted to 0.7 to 0.8 highlights the limit of the dissolution reactions unless Cr_2O_3 is dissolved to permit further FeO releases or Cr_2O_3 is exsolved from chromite in the form of eskolaite. Variations in Mg and Fe^{2+} are limited to about 0.1 fraction. These observations are not in line with the predicted equilibrium composition of chromite. As shown in Figure 8, equilibrium composition of chromite at 1300 °C in the presence of $CaCl_2$ is more Fe^{2+} rich with its Mg/(Mg+Fe^{2+}) ratio being 0.61 in comparison to the observed value of 0.77. The Mg/(Mg+Fe^{2+}) ratio of the ore only simulation at 1300 °C is 0.53 reflecting limited amount of FeO dissolution to the $CaCl_2$ melt. Changes in the chromite composition across the 800 to 1400 °C range are rather similar for the mixtures of ore+carbon and ore+carbon+flux.

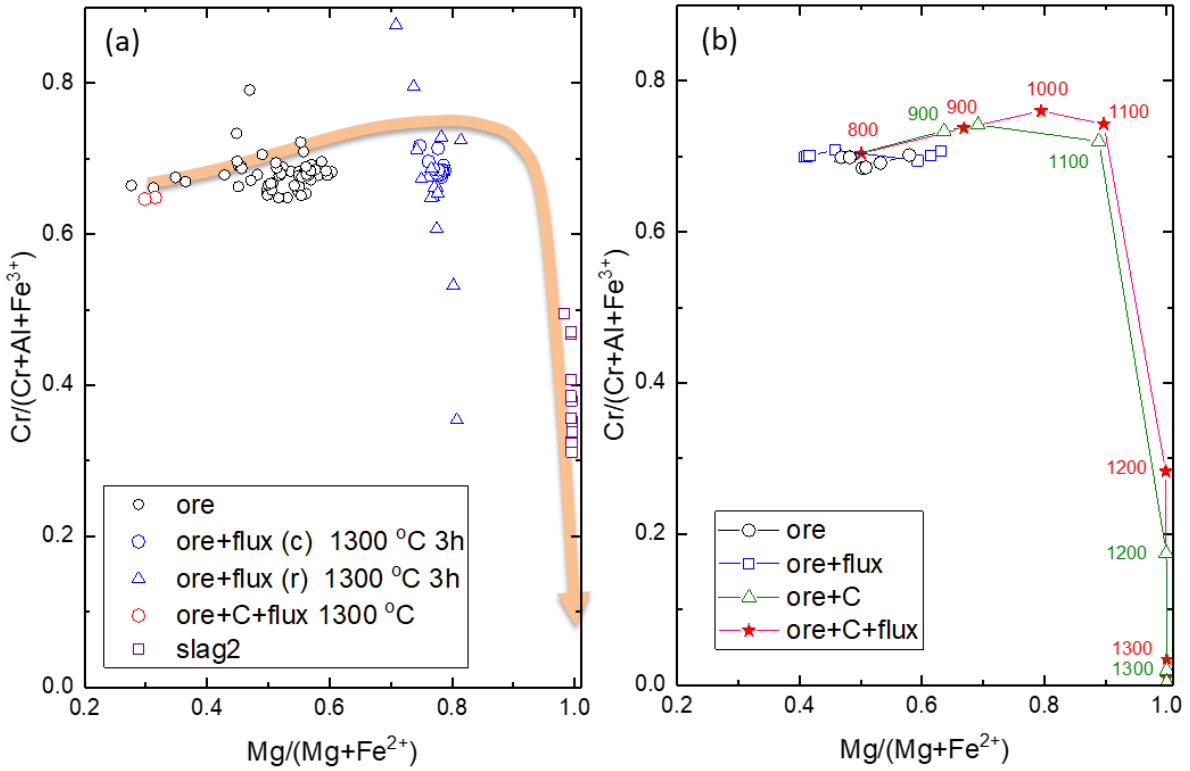

Figure 8. (a) Measured chromite compositions of ore (black), ore+$CaCl_2$ heated at 1300 °C for 3 hours (blue), ore+carbon+$CaCl_2$ heated to 1300 °C and cooled without dwell (red) and ore+carbon+$CaCl_2$+bentonite reduced at 1300 °C (purple). Core compositions of chromite shown in circles and those of their rims in triangles. Also shown is the overall reduction path in orange; (b) Equilibrium compositions of chromite at 800 to 1400 °C for ore (black), ore+$CaCl_2$(blue), ore+carbon (green) and ore+carbon+$CaCl_2$ (red) mixtures calculated by FactSage.

As illustrated in Figure 8, the reduction path is dominated by increases in the Mg/(Mg+Fe^{2+}) ratio during the early stages of reduction. This is accompanied by a slightly upward trend of increased Cr/(Cr+Al+Fe^{3+}) ratio due to reduction of Fe^{3+}. These changes continue until about 10 to 20 % Fe^{2+} remaining in the tetrahedral sites. At this point, the reduction path makes a sharp turn indicating the onset of Cr reduction with continual loss of Cr. All Fe^{2+} will have been reduced at about 30% Cr remaining in the octahedral sites. Following that, it is all Cr reduction until Cr is depleted.

Thermodynamic calculations predict that a slag liquid appears at 1250 °C forming 2.1 wt% of the products (Table 1). Its proportion increases to 7.4 wt% at 1400 °C. It seems that this increase counterbalances the decrease in the amount of molten salt at 1300 and 1400 °C. This slag liquid at 1300 °C is composed predominantly of SiO_2 (39.3 wt%), CaO (23.7 wt%), MgO (18.5 wt%) and Al_2O_3 (11.9 wt%). In addition, this slag liquid has about 6 wt% chlorides (i.e. 3.2 wt% $CaCl_2$ and 3 wt% $MgCl_2$); however, the chlorides soluble in the slag liquid form a very small proportion of the total chloride species in molten media (i.e. 0.9wt%). The weighted averages of the two liquids that are predicted to exist at 1300 °C indicate that the bulk liquid would consist predominantly of $CaCl_2$ (87.3 wt%) followed by 4.7 % SiO_2, 2.9 % CaO, 2.2 % MgO, 1.4 % Al_2O_3 and 1.3 % $MgCl_2$. The co-existing immiscible $CaCl_2$ salt liquid has 0.1 wt% CaO at 1300 °C and 0.4 wt% CaO at 1400 °C, indicating that the solubility of oxides in chloride salt is low. This is in line with Gordo et

al. (2004) in that molten $CaCl_2$ is incapable of dissolving the metal oxide; however, molten $CaCl_2$ has the capability of accommodating oxygen ions, in the form of associated or dissociated CaO. The thermodynamics predicts that the solubility of CaO in molten chloride increases with temperature (Table 1).

Iron is present as a chloride at temperatures of 800 to 1200 °C, forming between 3.5 and 13 wt% of the salt liquid suggesting that Fe can be carried as chloride complexes. At 1300 °C, slag liquid has trace concentrations of Fe (200 ppm as FeO) and Cr (3000 ppm dominantly as CrO). This is indicative of near complete reduction of Fe and Cr species upon reaching equilibrium. The presence of Cr in slag liquid as Cr^{2+} indicates that Cr is transported as divalent species in the melt at 1300 °C.

Table 1 – Equilibrium compositions of the slag and salt liquids at 1250, 1300 and 1400 °C predicted by FactSage

	1250 °C		1300 °C		1400 °C	
	slag	salt	slag	salt	slag	salt
wt% liq.	*10.1*	*89.9*	*12.0*	*88.0*	*32.5*	*67.5*
SiO_2	42.71		39.36		34.33	
Al_2O_3	13.72		12.02		7.33	
Cr_2O_3	0.01		0.01		0.01	
CrO	0.53		0.25		0.07	
FeO	0.04		0.02		0.01	
MgO	15.36		18.48		25.56	
CaO	22.77	0.05	23.63	0.10	22.74	0.42
$CaCl_2$	2.68	98.90	3.23	98.81	4.25	98.04
$MgCl_2$	2.16	1.04	3.01	1.08	5.70	1.53
$FeCl_2$	0.00	0.00	0.00	0.00	0.00	0.00
Total	99.98	99.98	100.01	99.99	100.00	99.99

Spinel, olivine, carbide and graphite are equilibrium phases. Note that slag liquid does not exist at 1200 °C.

Empirical data on slag compositions representing the direct reduction process are limited. A partially reduced sample heated up to 1300 °C without dwell and cooled down at the same rate (20 °C/min) produced a slag liquid composition that is composed of 42.16 wt% SiO_2, 33.91 wt% CaO, 9.58 wt% Al_2O_3, 9.81 wt% Cl, and 4.53 wt% MgO (Table 2). With the exception of MgO, its composition is comparable to the equilibrium slag liquid composition at 1300 °C (Table 1). Electron microprobe analyses of chromite particles indicate that there are no significant compositional changes from particle centers to rims. In essence, the slag would represent a reaction product of clinochlore, minor chromite and $CaCl_2$. It is a slow-cooled product; therefore, it is possible that exchange reactions and segregation occurred during cooling influencing the original equilibrium compositions. It appears that the oxide melt accommodates significant Cl. Another slag composition that resulted from an experiment with a slightly different feed composition is also comparable (shown as slag2 on Table 2). This is with the consideration of the differences in the feed composition and residual phases in the product. The feed of this slag contained 20 parts $CaCl_2$ and 4.7 wt% bentonite as a binder, and the residual spinel had significant Cr with the formula

of $MgAl_{1.2}Cr_{0.8}O_4$. An interesting observation is the presence of 3.46±0.30 wt% Cr_2O_3 in this slag. It is possible that the slag is in equilibrium with the residual Cr-spinel occurring as dispersed spongy particles in slag. This is in part due to the refractory nature and narrow compositional range of the residual Cr-spinel ($MgAl_{1.0\text{-}1.3}Cr_{0.6\text{-}1.0}O_4$). In this case, the Cr_2O_3 concentration of the slag can be representative of the solubility limit of this melt, although it would be slightly different for the typical DRC slag.

Table 2 – Observed and predicted equilibrium compositions of slag liquids (wt%)

	slag1			slag2
	observed	predicted		observed
	1300 °C	1250 °C	1300 °C	1300 °C
SiO_2	42.16	42.71	39.36	36.33
Al_2O_3	9.58	13.72	12.02	18.84
Cr_2O_3	0.69	0.60	0.29	3.46
FeO	0.20	0.04	0.02	0.06
MgO	4.53	16.27	19.76	1.58
CaO	33.91	24.11	25.25	34.28
Cl	9.81	3.34	4.32	4.04
Total	100.88	100.79	101.02	98.59

Slag1: 100:22:30; slag2: 100:22:20 with 4.7 wt% bentonite; observed slag compositions are based on EPMA.

In the absence of carbon, predicted slag liquid compositions at 1300 °C are broadly comparable to those discussed above (Table 3). This is with the exception of FeO and $FeCl_2$ since Fe is reduced in the presence of carbon. Slag and salt liquids form two separate immiscible melts in both case. The amount of slag liquid forming during reactions involving C is much lower in comparison to without C, which is about 4 times lower. There is a significant amount chlorides dissolved in the slag liquid in both cases. In contrast, there is very little to no oxygen dissolved in molten chloride.

Table 3 – Equilibrium compositions of slag and salt liquids in the absence and presence of carbon(1300 °C)

	ore+$CaCl_2$+C		ore+$CaCl_2$	
	slag	salt	slag	salt
wt% liq.	*12.0*	*88.0*	*41.0*	*59.0*
SiO_2	39.36		35.43	
Al_2O_3	12.02		8.99	
Cr_2O_3	0.01		0.06	
CrO	0.25		0.18	
FeO	0.02		17.35	
MgO	18.48		10.46	
CaO	23.63	0.10	17.81	
$CaCl_2$	3.23	98.81	3.76	100.00
$MgCl_2$	3.01	1.08	2.64	
$FeCl_2$	0.00	0.00	3.27	
Total	100.01	99.99	99.95	100.00

The glassy slag phase of the product that formed at 1300 °C after 3 hours of reaction of ore with $CaCl_2$ (100:30 proportion by mass) is similar in composition to wadalite ($Ca_6Al_5Si_2O_{16}Cl_3$) based on electron microprobe analyses (Table 4).

Table 4 – Electron probe microanalysis (EPMA) of slag (wt%)

	EPMA average	wadalite theoretical
SiO_2	11.63	15.1
Al_2O_3	33.08	32.1
Cr_2O_3	0.61	
FeO	1.76	
MgO	0.38	
CaO	42.92	42.3
Cl	11.71	13.4
	102.09	102.9

EPMA average represents 3 slag particles

Speciation of Cr in slag

Chromium speciation in the slag was determined by micro X-ray absorption spectroscopy (XAS) at the Advanced Photon Source. The slag is represented by a product that resulted from reducing a chromite ore, petcoke and $CaCl_2$ mixture at 1300 °C for 3 hours. A small amount of bentonite was added to the mixture as a binder with the proportions of the ore, petcoke, $CaCl_2$ and bentonite being 67.1, 14.8, 13.4 and 4.7 wt%, respectively.

X-ray absorption near edge structure (XANES and extended X-ray absorption fine structure (EXAFS) spectroscopy experiments were carried out at the insertion device beamline, 20-ID equipped with a confocal optics, allowing filtering of the signals to pre-determined depths within the sample. This provided 2 to 5 µm depth resolution with a 2.5 µm beam. Micro-XRF maps collected at the Cr edge shown in Figure 9 provide the distribution of Cr near the sample surfaces. Their similarity to the BSE images confirm that the signals from deeper parts of the sample were effectively filtered out (Fig. 9).

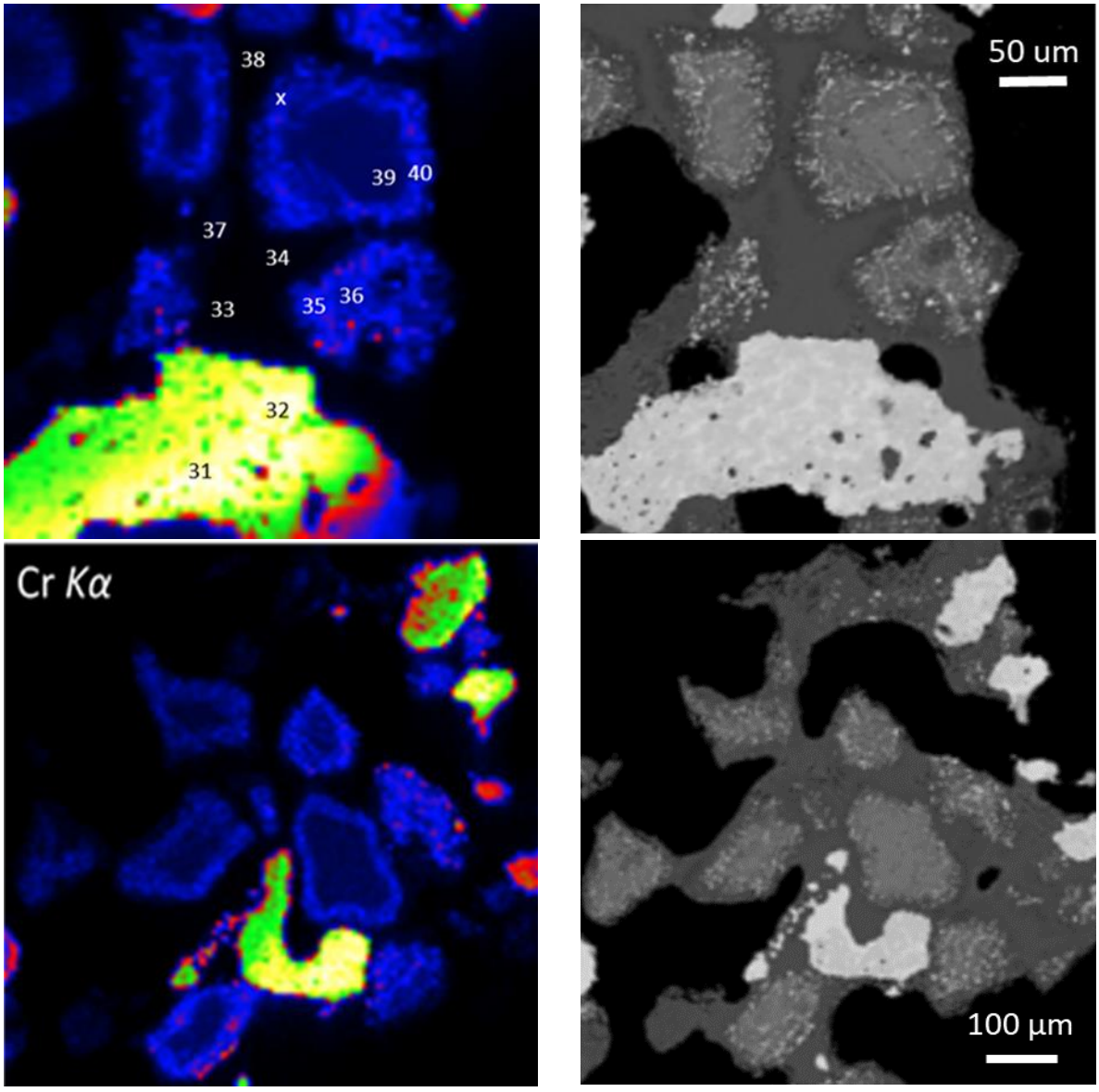

Figure 9. Micro-XRF images showing the distribution of Cr near the sample surfaces (left) with corresponding BSE images shown on the right. On the micro-XRF images, residual chromite particles appear as dark bluish black whereas the rims with disseminated FeCr alloy are bright blue. FeCr alloy occurs as green, yellow and red particles. Different Cr counts in FeCr particles reflect the Cr- and Fe-rich zones that exsolved from FeCr during cooling. Slag areas shown as dark grey areas in BSE photomicrographs have low Cr contents and appear as black background in the micro-XRF maps.

Cr K-edge micro-XANES spectra collected from the centres of residual chromite particles are identical to those that are typical of chromite (Fig. 10). This is also the case for the rims of the chromite particles; however, due to the abundance of disseminated FeCr particles in the rims, some spectra display features indicative of contamination from Cr^0 species. Ferrochrome where Cr is zerovalent has its main absorption edge at 5989 eV.

Micro-XANES spectra collected from the slag areas (i.e. matrix to residual chromite and alloy particles) and alloy are also shown in Figure 10a. The spectrum labeled "slag" is the most common slag type. The slag spectra are different from the others in that the absorption edge of the slag is at a lower energy position than the known species of Cr^{3+} like chromite, Cr_2O_3 and $CrCl_3$, and above Cr^0 (alloy) and $CrCl_2$ (Fig. 10b).

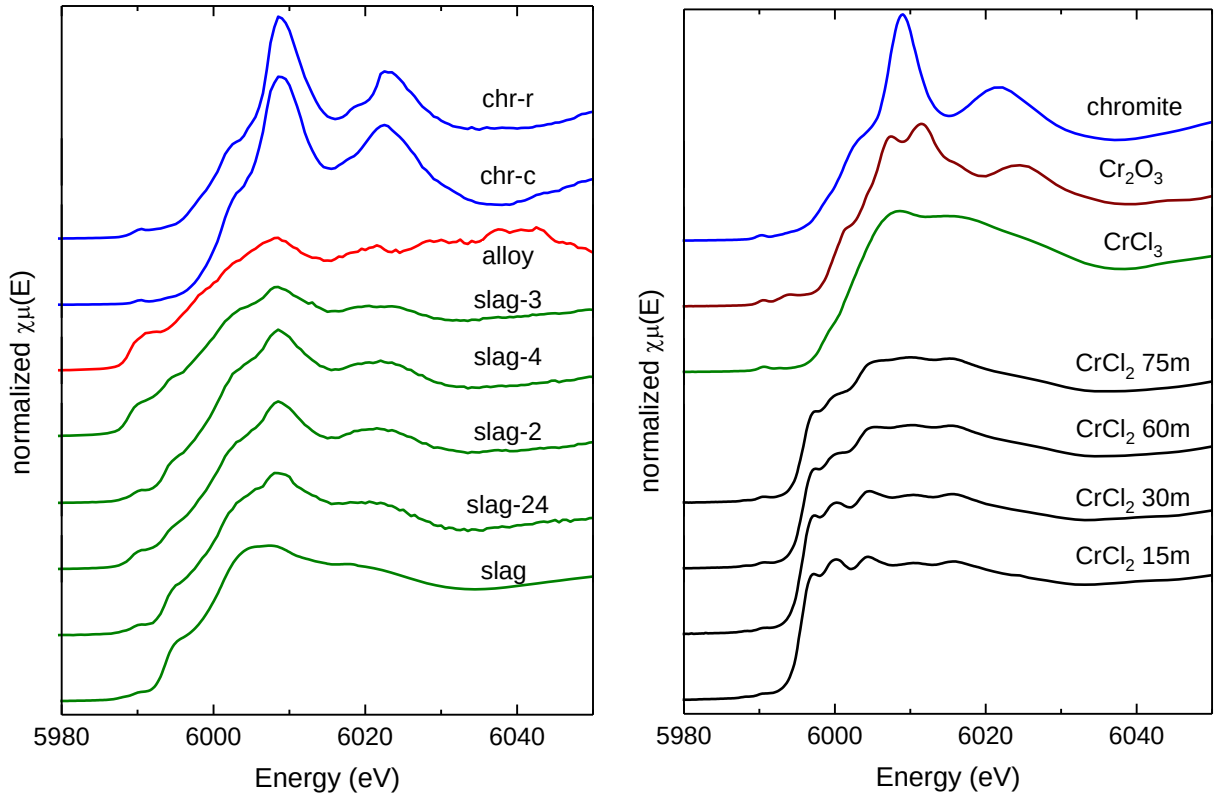

Figure 10. (a) Representative Cr K-edge micro-XANES spectra collected from various slag areas, residual chromite (chr-c: center and chr-r: rim) and alloy particles; (b) XANES spectra of relevant reference materials shown for comparison. Numbers next to $CrCl_2$ are minutes under which the $CaCl_2$ reference compound exposed to intense X-ray beam. The edge shifts to higher energies with exposure due to partial oxidation of Cr^{2+} to Cr^{3+}.

As shown in Figure 11, the derivative spectrum of the slag has two pre-edge features at 5989.5 and 5993.7 eV below the main peak at 6001.2 eV. These pre-edge features are assigned to 1*s*→3*d* and 1*s*→4*s* transitions as per Waychunas et al. (1983) and Sutton et al. (1993). The XANES region of the first-row transition elements is comprised of two pre-edge features several eV below the main absorption edge varying systematically in their energy position and intensity with valence, symmetry of the coordination environment and metal-ligand bond type (Waychunas et al., 1983). For instance, in the case of Fe as the absorber, a valence change from 3+ to 2+ corresponds to about -2 eV shift of the 1*s*→3*d* peak, and to about -2.4 eV shift of the 1*s*→4*s* feature (Waychunas et al., 1983). These are -1 and -2 eV shifts for changing from Cr^{3+} to Cr^{2+} in synthetic olivines (Sutton et al., 1993).

Relative to the 1*s*→3*d* peak, spectral features of the Cr^{2+} species in borosilicate glass and lunar olivine (Sutton et al., 1993) have energies of 4-5.5 eV for the 1*s*→4*s*, 11.5-14 eV for the main peak and 14-17.5 eV for the edge crest. These are 4, 11.9 and 18.9 eV for the silicate glasses of Berry and O'Neill (2004). In comparison, the slag has these spectral features at 4.2, 11.7 and 17.9 eV which are similar to those of the Cr^{2+} species in glasses indicating that Cr in the slag is in essence divalent (Fig. 11).

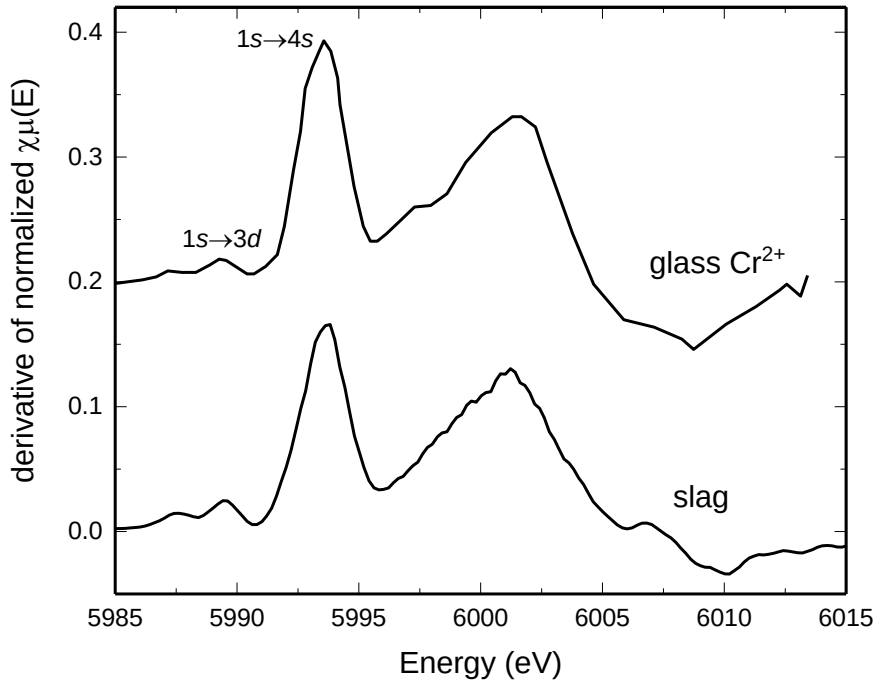

Figure 11. Derivative Cr K-edge XANES spectrum of the slag (slag-a) shown in comparison to that of Cr^{2+} glass of Berry and O'Neill (2004) (digitized spectrum shifted 1.5 eV to lower energies to line up with the 1*s*→3*d* peak of the slag). The slag has 1*s*→3*d*, 1*s*→4*s* and the main peaks at 5985.5, 5993.7 and 6001.2 eV, respectively.

Using the approach of Berry and O'Neill (2004) in integrating the area of 1*s*→4*s* peak and with the assumption that Cr^{2+} coordination environments in the reference glass and the slag are the same, the fraction of Cr^{2+} in the slag can be estimated as 0.9 of the total Cr present. The proportion of Cr^{2+} could be higher or entirely Cr^{2+} depending upon the compositional influence (the glass reference is on the anorthite-diopside eutectic involving CaO, MgO, Al_2O_3 and SiO_2) and partial oxygen pressure. Oxygen partial pressure under which the slag formed is estimated to be close to $1x10^{-16}$ atm, representing the C-CO equilibrium which would promote the highest proportion of Cr^{2+}in the slag. This finding is in agreement with the predicted equilibrium calculations at 1300 °C indicating that the proportion of Cr^{2+} to total Cr in melt is 0.96 (Table 3).

Some of the slag areas labeled with numbers like "slag-1" on Figure 10, are mixtures of the slag, chromite and alloy. Least squares fitting of the spectra indicated that such slags are composed of 26.8 to 91.2 % slag, 1.7 to 64.6 % alloy and up to 23.8 % chromite (Fig. 12 and Table 5).

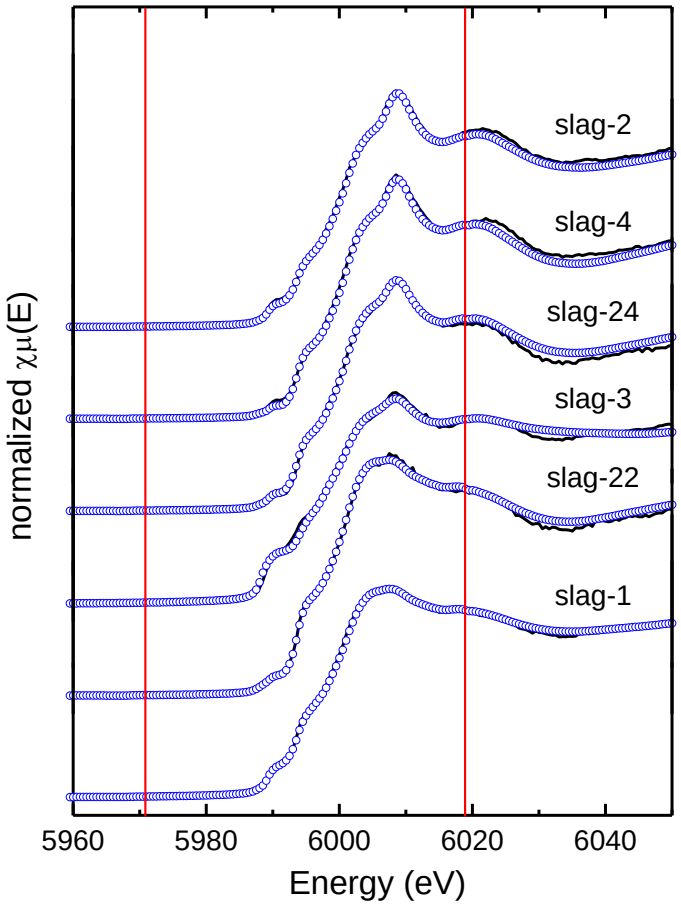

Figure 12. Linear combination fitting of the normalized Cr K-edge XANES spectra of the various slag areas using end-members of slag, chromite and alloy. Measured spectra shown in black solid lines and fitted spectra in blue circles. End-members are shown in Figure 10 and the fitting results in Table 5. Vertical red lines mark the fitting range of -20 eV to 30 eV.

Table 5. Proportions of slag, chromite and alloy determined by linear combination fitting of the spectra collected from various slag areas

	slag	chromite	alloy	R-factor	chi-square
slag-1	66.8		33.2	0.00018	0.0087
slag-2	54.5	23.8	21.7	0.00033	0.0156
slag-3	26.8	8.7	64.6	0.00080	0.0364
slag-4	74.8	23.5	1.7	0.00047	0.0239
slag-22	91.2		8.8	0.00025	0.0149
slag-24	73.3	16.9	9.9	0.00025	0.0119

Slag is represented by slag-a spectrum. R-factor and chi-square values are goodness-of-fit parameters

Local structure of Cr in slag

Chromium K-edge EXAFS spectra collected from the slag and various relevant reference materials are shown in Figure 13. The slag spectrum represents averages of scans collected from various parts of the slag areas forming the matrix to residual chromite and alloy particles as discussed earlier. Although the spectrum is noisy, oscillations are resolvable for the k range up to about 11 $Å^{-1}$ for determining the local structures. The spectrum is broadly different from the spectra of the reference species of Cr^{3+}, Cr^{2+} and Cr^{0}. First, the spectrum was simulated within the k range from 3 to 11 $Å^{-1}$ by various combinations of first shell paths of Cr-O and Cr-Cl. The best fit was obtained by a split 2 shells of oxygen atoms at radial distances of 1.95 and 2.11 Å. Corresponding coordination numbers were 1.6 and 2.4 totaling 4 oxygens. The quality of the fit is reasonable judging visually from the Fourier transform (Fig. 14) and the goodness-of-fit parameters (Table 6). Addition of Cr-Cr paths was not successful in simulations, corroborating the absence of higher shell neighbor atoms from the Fourier transform of the spectrum (Fig. 14). An examination of the reference materials indicated that all have one or more neighbor atoms beyond the first shell with high enough amplitudes above the Fourier transform ripples. This suggests that Cr occurs in slag in four-fold coordination. This coordination is judged to be planar rather than tetrahedral due to the absence of the pre-edge peak at ~5989 eV (1s→3d transition) which is a diagnostic marker of tetrahedral Cr^{6+} (Peterson et al., 1997; Zachara et al., 2004; Berryman and Paktunc 2021), and the shorter Cr-O distances of tetrahedral Cr (i.e. 1.59-1.85 Å). The planar four-fold coordination is analogous to the CrO compounds where the Cr-O distances are around 2 Å (Barin 1996).

Table 6. Local structural parameters of the slag determined from fitting of Cr K-edge EXAFS spectrum

	CN	*R*	σ^2	E0	rf	chi-sq
Cr-O1	1.6±0.4	2.11	0.0016	3.9	0.028	6676
Cr-O2	2.4[a]	1.95	0.0016[b]			

CN: coordination number; R interatomic distance (Å); σ^2: Debye-Waller parameter ($Å^2$); E0: energy offset (eV); rf (r-factor) and chi-sq (chi square) as the goodness-of-fit parameters. Fit performed in R-space with R=1-3 Å, k=3-11 $Å^{-1}$ and amplitude-reduction factor (S_0^2) constrained to 0.9; [a] fixed as 4-CN(O2); [b] fixed as σ^2(O1). Number of independent points/number of variable value is 9.9/5.

In the absence of 2nd shell atoms, it is concluded that Cr-O occurs in the form of monomers, probably afforded by the dilute nature of Cr in the slag. Electron microprobe analyses indicate that CrO content of the slag is relatively uniform at 3.10±0.27 wt%, forming the soluble fraction of slag at 1300 °C. The slag is dominated by SiO_2, CaO and Al_2O_3 (i.e. 36.33 wt%, 34.28 wt%, 18.84 wt% respectively) with minor Cl at 4.04±0.18 wt% and MgO at 1.58±0.26 wt%. In this case, it is contemplated that Cr is transported in the slag as ionic species that are four-fold coordinated to oxygen forming monomers. The findings also indicate that Cr was reduced to Cr^{2+} in the melt before it reached to solid carbon particles.

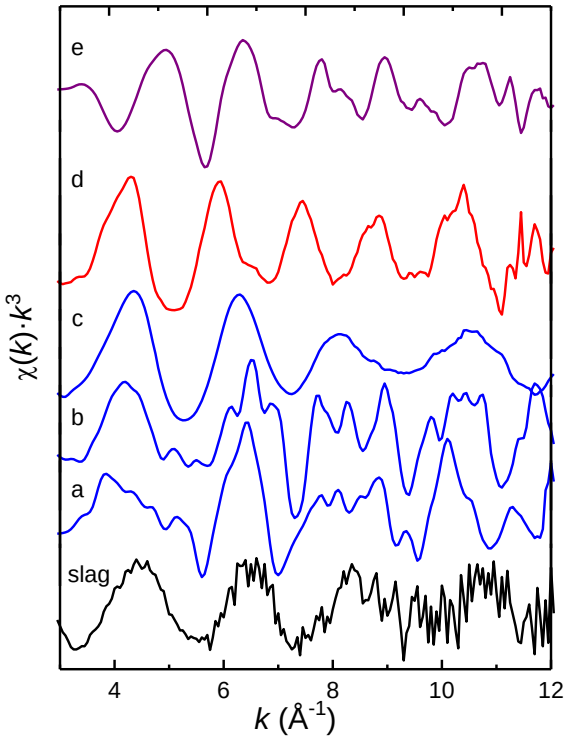

Figure 13. Chromium K-edge EXAFS spectra of the slag and reference compounds of chromite (a), Cr_2O_3 (b), $CrCl_3$ (c), $CrCl_2$ (d) and Cr_3C_2 alloy (e).

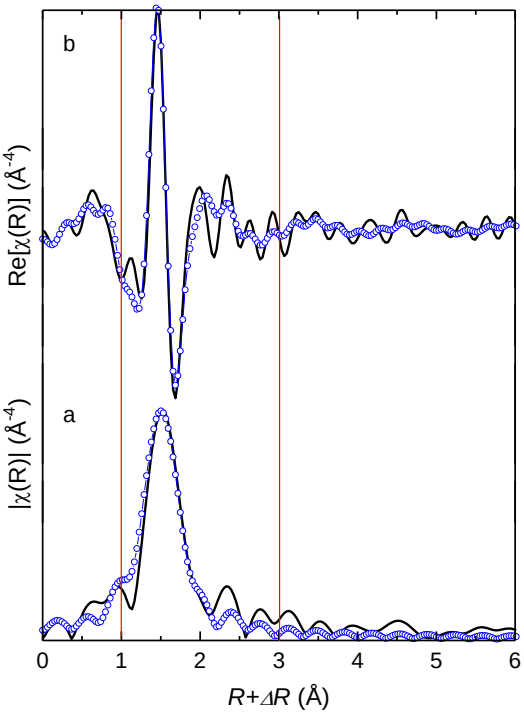

Figure 14. Fourier transform (a) and real part (b) of the Cr K-edge EXAFS spectrum of the slag and its fit. Experimental spectrum shown in solid black line and fit in blue circles. Fitting was performed within 1-3 Å as marked by red lines.

Mechanism of the process

The mechanism of DRC involves three processes: (1) dissolution of chromite, (2) transport of dissolved Cr and Fe species in molten media and (3) reduction on carbon particles as a Cr-Fe alloy as illustrated in Figure 15. Dissolution of chromite in molten $CaCl_2$ can be described by the following reaction (18) where the reducible cations are depicted as dissolved Cr_2O_3 (ℓ) and FeO (ℓ) species in melt:

$$Mg_{0.4}Fe_{0.6}Cr_{1.4}Al_{0.6}O_4 + CaCl_2(\ell) \rightarrow 0.7\ Cr_2O_3(\ell) + 0.6\ FeO(\ell) + 0.3\ MgAl_2O_4(s) + 0.1\ MgO(s) + CaCl_2(\ell) \quad (18)$$

As the reaction proceeds, beginning at particle margins, chromite shrinks by leaving behind refractory spinel ($MgAl_2O_4$) which has a porous morphology. The dissolved species are transported in the molten media through the porous spinel to carbon particles. In this regard, the DRC process would be analogous to an electrolytic cell where carbon and chromite form the electrodes and molten $CaCl_2$ the electrolyte where the reduction of iron and chromium oxide species are represented by the following reaction steps:

$$FeO + 2e \rightarrow Fe + O^{2-} \quad (19)$$

$$Cr_2O_3 + 2e \rightarrow 2CrO + O^{2-} \quad (20)$$

$$CrO + 2e \rightarrow Cr + O^{2-} \quad (21)$$

$$Cr_2O_3 + 6e \rightarrow 2Cr + 3O^{2-} \quad (22)$$

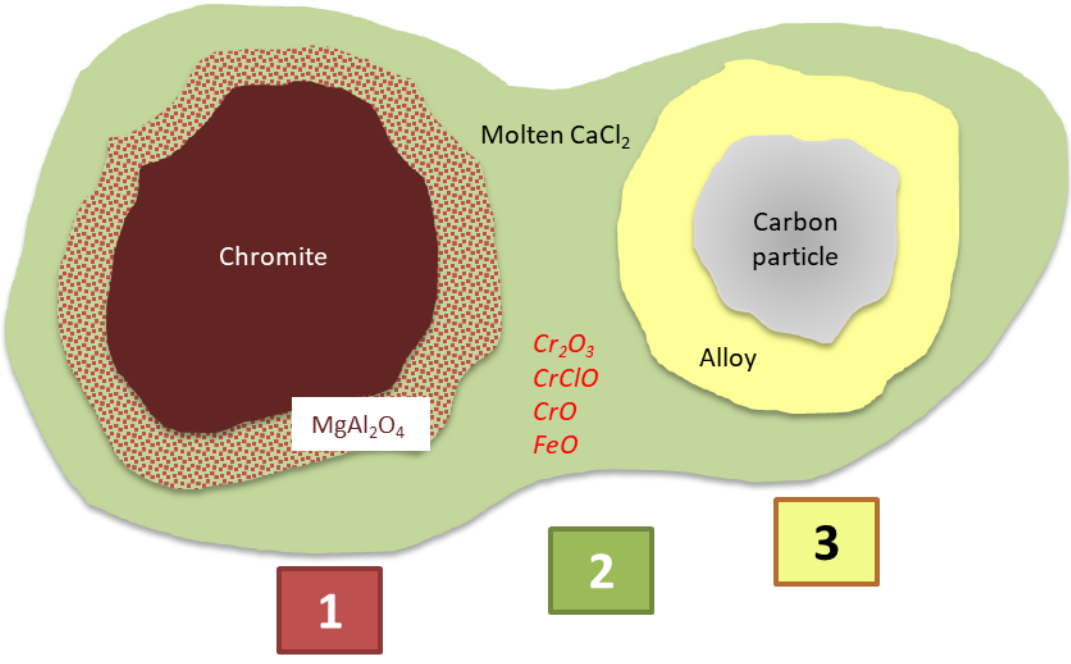

Figure 15. A cartoon illustration of the mechanism of the $CaCl_2$-assisted DRC process. (1) incongruent dissolution of chromite leaving behind solid refractory spinel ($MgAl_2O_4$); (2) transport of dissolved Cr and Fe species from chromite to carbon particle through molten $CaCl_2$; (3) reduction reactions on carbon particles and growth of Cr-Fe alloy.

The overall reaction is driven by the concentration gradient between chromite and carbon particles across the molten salt solution, which would require chemical reactions to be faster at reduction sites. Upon reaching the reductant particles, Cr and Fe are reduced resulting in the formation of Fe-Cr alloy which grows at the expense of the carbon particle by moving closer to the centre of the core. In essence, these reactions can be described as shrinking cores of chromite and reductant particles occurring in unison as the reactions proceed (Fig. 16).

There appears to be two critical factors controlling the fate of direct reduction of chromite ores. The first is the composition and mineralogical properties of the gangue minerals, especially if they melt at temperatures before reduction reactions begin. When flux melts at ~760 °C to form a liquid layer around chromite particles and acting as a liquid bridge between chromite and reductant particles, its composition evolves with time not only with the Fe and Cr as ionic species coming from the dissolution of chromite but also with the species contributed from melting of the gangue minerals. The melt must be able to accommodate Fe and Cr species in solution (i.e. solubility) until they reach reduction sites. The second factor is the viscosity of the melt, which makes the mass transport or diffusion of Fe and Cr species possible from the dissolving chromite surfaces to carbon particle surfaces where reduction occurs.

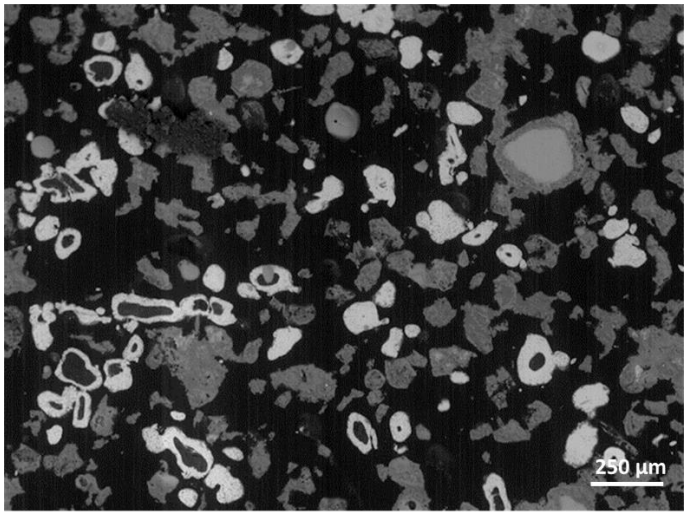

Figure 16. Backscattered electron micrograph showing shrinking cores of chromite and petcoke particles. A large chromite particle (light grey) on the right is enveloped by residual Mg-Al spinel (dark grey) outlining the original chromite particle. Very dark to black particles surrounded by white particles (ferrochrome) are residual petcoke. Black background/matrix material is epoxy. With continued reduction all chromite and petcoke centers shrink and disappear.

The dissolution of chromite is controlled by the solubility limits of Cr and Fe in molten salt. It requires that the melt remains undersaturated with respect to Fe and Cr. As discussed earlier, molten salt has low solubilities of oxides; however, thermodynamics predict that iron can be present as chloride complexes, forming between 3.5 and 13 wt% of the salt liquid at temperatures of 800 to 1200 °C. According to Huang et al. (2019), Cr solubility is dependent on partial oxygen pressure, and the concentration of Cl^- ions in that large concentration of Cr can be transported at Cl^- rich fluids and under reducing conditions. Considering that local oxygen potential near the dissolving chromite surfaces is close to that of the CO-

CO_2 equilibrium whereas the local oxygen potential is much lower near the reductant surfaces close to the C-CO equilibrium as discussed by Yu and Paktunc (2018b), there is the possibility that not only Fe but also Cr species can be transported in molten chloride as ionic complexes. This would be limited to about 1200 °C for Fe as chloride complexes as per the thermodynamic predictions.

There are two reactions occurring simultaneously: one at the source where chromite is dissolving and the other at the reduction site where Cr and Fe species are being reduced to form M_7C_3 alloy. Consumption of the dissolved species of Fe and Cr on carbon/alloy particles would be the driving force behind the transport or diffusion of the species in molten salt. This is because there is no active mixing of the molten media, which would be required to effectively mass transport or diffuse the dissolved species from near the chromite particles. The second reaction at the reduction sites has to be faster than the chromite dissolution reaction to keep the molten $CaCl_2$ undersaturated with respect to Fe and Cr. This would be analogous to a conveyor belt operating between dissolving chromite and reduction sites of carbon particles where Fe and Cr are reduced and taken from the melt. The dissolution, transport and reduction processes must operate in unison for the process to continue. If the transport is not fast enough due to viscosity of the melt or the reduction reactions are slow, the melt can reach saturation with respect to Fe and Cr species, which would result in the formation of Fe and/or Cr compounds.

As illustrated in Figure 17, incongruent dissolution of chromite begins at time 0 with an increase in Fe and Cr concentrations in molten $CaCl_2$. After about 1 hour, with the temperature reaching 1000 °C, Fe begins to reduce which would result in an increase in the Cr/Fe ratio of the melt. Until about 1200 °C, Fe reduction dominates the reactions, which would result in an exponential increase in the Cr/Fe ratio of the melt. At 1200 °C, Cr begins to reduce keeping the Cr concentrations of the melt below the saturation. Between 1 and 3 hours, the “conveyor belt” is in operation with the Cr and Fe species being transported from dissolving chromite particles to reduction sites on carbon particle surfaces. This keeps the concentration of dissolved species below the saturation limit (equilibrium). Studies indicate that after 2 hours of reduction at 1200 °C, 92% of Fe and 59% of Cr are reduced. As the temperature reaches 1300 °C, all the Fe species are reduced and reactions would involve only Cr reduction. At 1300 °C, about 95% Cr metallization is achieved after 2 hours. At time 3, carbon is depleted and if there is still chromite present, the concentration of dissolved species increase until time 4 is reached where the liquid is saturated with respect to Cr (and/or Fe depending upon the temperature) and the reactions stop.

Based on the average of four thermocouple measurements made from different parts of a large crucible, it takes on average about 37 minutes to reach 1100 °C from 1000 °C, 39 minutes from 1100 to 1200 °C and 54 minutes from 1200 to 1300 °C. These temperature gradients are indicative of the increasingly endothermic nature of the reduction reactions with the onset of Cr reduction. In essence, it takes little more than 2 hours to reach the reduction temperature of 1300 °C. With another 2-h hold time at 1300 °C, the overall time needed in the furnace for complete metallization would be 4 hours.

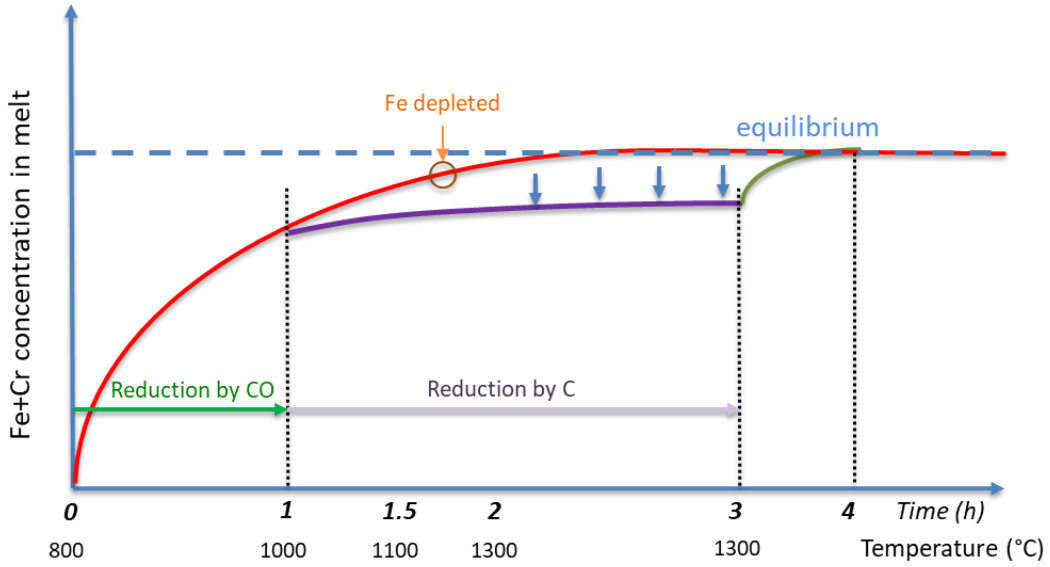

Figure 17. Conveyor belt analogy depicting the solubility limit of Fe or Cr species in molten $CaCl_2$ with time.

It is conceptualized that the overall rate control is the chemical reactions on chromite particles that is the incongruent dissolution of chromite. The dissolved species are then transported to reduction sites. Once the dissolved species reach carbon, they are reduced and taken away from the melt with the diffusion of the species across the alloy particle (molten or semi-molten). As the alloy rim grows at the expense of the carbon particle shrinking, diffusion of species across the alloy may become the rate-limiting step, especially towards the final stages where the alloy rim thickens. In fact, it appears that this is what is happening based on the evolution of off-gas composition evidenced from the experiments conducted at temperatures 1400 °C and above. (Carter et al., 2021).

SUMMARY

Chromite can be direct-reduced with the use of fluxes such as NaOH, cryolite (Na_3AlF_6) and $CaCl_2$ at temperatures that are much lower than those of smelting in electric arc furnaces. Reaction times of about 2 hours at 1300 °C are sufficient to form an M_7C_3 type carbide with Cr/Fe ratios that are close to those of the original chromite indicating high degrees of metallization. Ferrochrome particles are separated from the slag, which is dominated by refractory Mg-Al spinel through conventional mineral processing techniques such as gravity and magnetic techniques.

The reactions begin with the reduction of Fe^{3+} and Fe^{2+} species by CO, which results in the formation of Fe-rich alloy particles in-situ within chromite. The early stages of reduction are controlled by chemical reactions on the surfaces of chromite (i.e. dissolution of Fe and Cr from chromite by molten $CaCl_2$) under low partial pressures of oxygen close to that of the CO-CO_2 equilibrium. Incongruent dissolution starting from the margins of chromite particles gradually moves inward leaving behind a refractory spinel dominated by Mg and Al. Chromite compositional changes involve Mg-Fe^{2+} exchange reaction with gradual increases in the proportion of Mg until about 10 to 20 % Fe^{2+} remaining in the tetrahedral sites. From about 1100 to 1200 °C, the remaining Fe and 70% of Cr are reduced. This is followed by the reduction of the residual Cr in Mg-Al spinel at 1300 °C. Dissolved Fe and Cr species are carried from chromite to

reductant particles as ionic species in melt. Speciation and local structural data indicate that Cr is transported in melt as monomeric species of CrO in a four-fold coordination, already reduced to Cr^{2+}. The rate control may change with time, influenced by the variations in the composition of the melt, polymerization of the ionic species and the viscosity of the melt. It is conceptualized that the overall rate control is the chemical reactions on chromite particles that is the incongruent dissolution of chromite. As the alloy rim grows at the expense of the carbon particle shrinking, diffusion of species across the alloy (molten or semi-molten) may become the rate-limiting step, especially towards the final stages with the alloy rim thickens.

ACKNOWLEDGEMENT

The study has benefited from contributions and discussions with Drs. Dawei Yu, Samira Sokhanvaran, Nail Zagrtdenov, David Carter and Jason Coumans. The study is funded by Natural Resources Canada's REE and Chromite Initiative. The XANES and EXAFS measurements at APS were carried out under a General User Proposal and a Partner User Proposal supported by the Natural Sciences and Engineering Research Council (NSERC) of Canada through a major facilities access grant. Research at the PNC–CAT beamline of APS, Argonne National Laboratory, is supported by the U.S. Department of Energy under Contracts W–31–109–Eng–38 (APS) and DE–FG03– 97ER45628 (PNC–CAT).

REFERENCES

Barin I (1996) Thermochemical Data of Pure Substances. Third Edition, Two Volumes. Vol. 1: Ag-Kr and Vol. II: La-Zr. J. Am. Chem. Soc., 118, 39, 9459 https://doi.org/10.1021/ja965624c

Barnes AR, Muinonen M, Lavigne MJ (2015) Reducing energy consumption by alternative processing routes to produce ferrochromium alloys from chromite ore. Proceedings of COM 2015. The Metallurgical Society of CIM. pp. 1–22.

Berry AJ and O'Neill HSC (2004) A XANES determination of the oxidation state of chromium in silicate glasses. American Mineralogist, 89, 790–798.

Berryman E and Paktunc D (2021) Cr(VI) formation in ferrochrome-smelter dust. Journal of Hazardous Materials 422, 126873. https://doi.org/10.1016/j.jhazmat.2021.126873

Carter D, Coumans J, Zagrtdenov N, Paktunc D (2021) Optimization of pellet properties and reduction performance of the DRC process. CanmetMINING Technical Report, Chromite R&D Initiative, Chapter 3.2.6.11, 101p.

Coumans J, Carter D, Paktunc D, Zagrtdenov N (2021) Kinetic investigation of Direct Reduction Chromite (DRC): an application of the grain model. CanmetMINING Technical Report, Chromite R&D Initiative, Chapter 3.2.6.12, 22p.

Gordo E, Chen GZ, Fray DJ (2004) Toward optimisation of electrolytic reduction of solid chromium oxide to chromium powder in molten chloride salts. Electrochimica Acta 49, 2195-2208.

Hatch (2016) Summary and Analysis of the Current State of Developments for the Exploitation of the Ring of Fire Deposits and Opportunities for Downstream Value. Natural Resources Canada Engineering Report, R&D Gap Analysis for the Development of the Ring of Fire Chromite Deposits H351079-00000-210-230-0002, 30p.

Huang J, Hao J, Huang F, Sverjensky DA (2019) Mobility of chromium in high temperature crustal and upper mantle fluids. Geochemical Perspectives Letters 12, 1-6, doi: 10.7185/geochemlet.1926

International Chromium Development Association (2016) Life Cycle Inventory (LCI) of Primary Ferrochrome Production 2012. International Chromium Development Association. 48p.

Paktunc D (2021) Chromite R&D Initiative – Background, Objectives, Approach and Summary of Accomplishments. CanmetMINING Technical Report, Chromite R&D Initiative, Chapter 1.1, 19p.

Paktunc D, Thibault Y, Sokhanvaran S, Yu D (2018) Influences of alkali fluxes on direct reduction of chromite for ferrochrome production. The Journal of the Southern African Institute of Mining and Metallurgy 118: 1305-1314. http://dx.doi.org/10.17159/2411-9717/2018/v118n12a9

Peterson ML, Brown GE, Parks GA, Stein CL 1997 GCA Differential redox and sorption of Cr(III/VI) on natural silicate and oxide minerals: EXAFS and XANES results. Geochimica et Cosmochimica Acta, 61, 3399-3412.

Sokhanvaran S, Paktunc D (2017) The effect of fluxing agent on direct reduction of chromite ore. Proceedings of COM 2017. Canadian Institute of Mining, Metallurgy and Petroleum, Vancouver

Sokhanvaran S, Paktunc D (2019) Method of direct reduction of chromite with cryolite additive. US Patent, US10358693B2, July 23, 2019.

Sokhanvaran S, Paktunc D, Barnes A (2018) NaOH–assisted direct reduction of Ring of Fire chromite ores, and the associated implications for processing. The Journal of the Southern African Institute of Mining and Metallurgy 118: 581-588. http://dx.doi.org/10.17159/2411-9717/2018/v118n6a4

Waychunas GA, Apted MJ, Brown GE (1983) X-Ray K-Edge Absorption Spectra of Fe Minerals and Model Compounds: Near-Edge Structure. Physics and Chemistry of Minerals, 10, 1-9

Winter F (2015) Production of chromium iron alloys directly from chromite ores. US patent US2016/0244864 A1.

Yu D, Paktunc D (2018a) Carbothermic direct reduction of chromite using a catalyst for the production of ferrochrome alloy. Patent. World Intellectual Property Organization, WO2018/201218A1.

Yu D, Paktunc D (2018b) Calcium chloride-assisted segregation reduction of chromite: Influence of reductant type and the mechanism. Minerals 8: 45 (Special Issue "Towards Sustainability in Extractive Metallurgy", Ed. Chris Pickles). https://doi.org/10.3390/min8020045

Yu D, Paktunc D (2018c) Direct production of ferrochrome by segregation reduction of chromite in the presence of calcium chloride. Metals 8: 69. https://doi.org/10.3390/met8010069

Zachara, J.M., Ainsworth, C.C., Brown, G.E., Catalano, J.G., McKinley, J.P., Qafoku, O., Smith, S.C., Szecsody, J.E., Traina, S.J., Warner, J.A., 2004. Chromium speciation and mobility in a high level nuclear waste vadose zone plume. Geochimica et Cosmochimica Acta, 68, 13-30.